

# Stellar population analysis on the stacked spectra of double-peaked emission-line galaxies

Meng-Xin Wang<sup>1,2</sup> and A-Li Luo<sup>1,2,3</sup>

<sup>1</sup> National Astronomical Observatories, Chinese Academy of Sciences, Beijing 100101, China; [lal@nao.cas.cn](mailto:lal@nao.cas.cn)

<sup>2</sup> University of Chinese Academy of Sciences, Beijing 100049, China

<sup>3</sup> Department of Physics and Astronomy, University of Delaware, Newark, DE 19716, USA

Received 2018 October 9; accepted 2019 April 9

**Abstract** Double-peaked emission-line galaxies have long been perceived as objects related to merging galaxies or other phenomena with disturbed dynamical activities, such as outflows and disk rotation. In order to find the connection between the unique activities happening in these objects and their stellar population physics, we study the stellar populations of the stacked spectra drawn from double-peaked emission-line galaxies in the Large Sky Area Multi-Object Fiber Spectroscopic Telescope (LAMOST) Data Release 4 (DR4) and the Sloan Digital Sky Survey (SDSS) Data Release 7 (DR7) databases. We group the selected double-peaked emission-line objects into 10 different types of pairs based on the Baldwin-Phillips-Terlevich (BPT) diagnosis for each pair of blueshifted and redshifted components, and then stack the spectra of each group for analysis. The software STARLIGHT is employed to fit each stacked spectrum, and the contributions of stars at different ages and metallicities are quantified for subsequent comparative study and analysis. To highlight the commonality and uniqueness in these double-peaked emitting objects, we compare the population synthesis results of the stacked spectra of double-peaked emission-line galaxies with those of their counterpart reference samples displaying single-peaked emission features. The reference samples are also selected from the LAMOST DR4 and SDSS DR7 databases. From the comparison results, we confirm the strong correlations between stellar populations and their spectral classes, and find that the double-peaked emitting phenomenon is more likely to occur in an ‘older’ stellar environment and the subgroups hosting different BPT components will show an obvious heterogeneous star formation history.

**Key words:** galaxies: evolution — galaxies: stellar content

## 1 INTRODUCTION

In recent years, with the advent of large-scale spectroscopic surveys of galaxies, more efforts have been invested in the search for double-peaked narrow emission line galaxies, which were usually considered to be associated with merging galaxies or even dual active galactic nuclei (AGNs) (e.g., Wang et al. 2009; Liu et al. 2010; Smith et al. 2010; Ge 2012). As has been proved in previous works (e.g., Wang et al. 2009; Blecha et al. 2013), if two galaxies merge at kiloparsec (kpc) scale, and the adjacent narrow emission lines emitted are detected by a single spectrograph slit or fiber, double-peaked narrow emission line features would appear in the spectra. Follow-up observations of the reported double-peaked emission-line candidates have revealed that the confirmation rate

is low (e.g., Shen et al. 2011; Comerford et al. 2012), which seems to conflict with expectations inferred from the galaxies’ merging rate and the triggering of gas accretion onto black holes during the merging stage (e.g., Springel et al. 2005; Hopkins et al. 2005; Van Wassenhove et al. 2012). Based on the observationally estimated major merger rates of galaxies, and various scaling relations on the properties of galaxies and their central massive black holes, Yu et al. (2011) suggested a phenomenological model to estimate the number density of dual AGNs and its evolution. The confirmation of kpc-scale binary or dual AGN systems from the selected double-peaked candidates still verifies the reliability of systematic searches based on double-peaked criteria (e.g., Liu et al. 2013; Comerford et al. 2015). For instance, Liu et al. (2013) confirmed the binary-AGN scenario for two targets with high-resolution

optical and X-ray imaging from a parent sample of 167 Type II AGNs with double-peaked narrow emission lines selected from the Sloan Digital Sky Survey (SDSS; York et al. (2000)), and Comerford et al. (2015) identified six dual AGNs and dual/offset AGNs using X-rays based on a parent sample of 340 double-peaked emission-line AGNs identified in SDSS. Past research studies have also revealed that other processes not associated with merging galaxies or dual AGNs can also produce the phenomenon of narrow double-peaked emission, such as the disturbed narrow emission line regions (NLRs) involving biconical outflows (e.g., Gelderman 1994; Fischer et al. 2011; Shen et al. 2011; Fu et al. 2012; Nevin et al. 2018), the rotation-dominated regions with disturbance or obscuration (e.g., Nevin et al. 2016; Müller-Sánchez et al. 2015), and the local interaction of radio jets with NLR clouds (e.g., Rosario et al. 2010). Using spatially resolved information from long-slit data, Nevin et al. (2016) pinpointed the origin of NLRs for a complete sample of 71 Type II AGNs at  $z < 0.1$  with double-peaked features from the SDSS, and proposed a kinematic classification technique to discuss the scenarios that cause double-peaked emission lines in nearby galaxies. Based on a kinematic classification scheme and the follow-up optical long-slit observations of a sample of 95 SDSS galaxies that have double-peaked narrow AGN emission lines, Comerford et al. (2018) confirmed that the majority of double-peaked narrow AGN emission lines is associated with outflows, and eight of these targets are compelling dual AGN candidates and galaxies with double-peaked narrow AGN emission lines occur in such galaxy mergers at least twice as often as typical active galaxies.

The spectra of galaxies hold useful information on stellar ages and, more valuable, on the stellar metallicity distributions of their composed stellar populations. To comprehend the stellar populations of diverse galaxies, we need to retrieve the stellar compositions of a galaxy from its integrated spectrum, which is never an easy task. Stellar population synthesis on galaxies is developed as a means of estimating the physical properties of galaxies. The first group pioneered the empirical population synthesis method (Faber 1972), in which the integrated light of a galaxy can be reproduced by a linear combination of elements with known characteristics, such as the spectra of individual stars or star clusters exhibiting diverse ages and metallicities from the spectral library. A further group introduced the so-called evolutionary population synthesis methods relying mainly on models (e.g., Tinsley 1978; Bruzual A. 1983; Charlot et al. 1996; Bruzual & Charlot 2003, hereafter BC03), which follow the time evolution of the stellar system, and the parameters considered include

the stellar initial mass function (IMF), star formation rate and chemical history. As we have seen, the latter technique received more widespread adoption (e.g., Bressan et al. 1996; Vazdekis & Arimoto 1999; Le Borgne et al. 2004). Some works have emphasized the investigation of stellar populations on star-forming (SF) and starburst galaxies using optical data (e.g., Schmitt et al. 1996; Fernandes et al. 2003), and some works have been dedicated to research with AGNs, such as a series of stellar population analyses conducted on low-luminosity AGNs by Cid Fernandes et al. (2004, 2005a). In recent years, thanks to the explosion of integral-field spectroscopic (IFS) surveys, astronomers have the opportunity to fully characterize the properties of galaxies at different redshifts with better spatial resolution. Kuntschner et al. (2010) presented a stellar population analysis of the absorption line strength maps for 48 early-type galaxies from the Spectrographic Areal Unit for Research on Optical Nebulae (SAURON, Emsellem et al. 2007) sample. They have estimated the simple stellar population (SSP)-equivalent age, metallicity and abundance ratio  $[\alpha/\text{Fe}]$  over a two-dimensional field extending up to approximately one effective radius, with help from properties of  $\text{H}\beta$ ,  $\text{Fe}5015$  and  $\text{Mg b}$  measured in the Lick/IDS system. Mallmann et al. (2018) studied the effects of active nuclei on the star formation history of their host galaxies, by presenting spatially resolved stellar population age maps, average radial profiles and gradients for the first 62 AGNs observed with the SDSS-IV Mapping Nearby Galaxies at Apache Point Observatory (MaNGA, Bundy et al. 2015). Based on data from the Multi Unit Spectroscopic Explorer (MUSE, Bacon et al. 2015), Vaughan et al. (2018) measured the low-mass stellar IMF, and a number of individual elemental abundances, as a function of radius in NGC 1399, which is the largest elliptical galaxy in the Fornax Cluster. As for the merging galaxies, with which the double-peaked emission-line galaxies probably relate, some research on their stellar populations already exists. Barrera-Ballesteros et al. (2015) studied the impact of the interaction between specific star formation and oxygen abundance on different galactic scales, using the optical IFS data from 103 nearby galaxies at different stages in the merging event, from close pairs to merger remnants provided by the Calar Alto Legacy Integral Field Area (CALIFA, Sánchez et al. 2012) survey.

In the last decade, the relative abundance of multi-fiber spectrographs makes it feasible to obtain large amounts of spectra, and a large sample of double-peaked emission-line galaxies has been established. Ge (2012) conducted a systematic search to build the largest sample of 3030 double-peaked emission line galaxies from the SDSS Data Release 7 (DR7; Abazajian et al. 2009) database, and

Wang et al. (2019) also compiled a sample of 325 objects displaying double-peaked narrow line features based on the Large Sky Area Multi-Object Fiber Spectroscopic Telescope (LAMOST) Data Release 4 (DR4) data set. The present sample from large-scale spectroscopic surveys enables us to probe the influence of these unique dynamical activities on the stellar populations of these objects, and learn more about the relationship between nuclear activity and star formation history in the inner regions of AGNs, which is one crucial question in galaxy formation and evolution research. In this work, we will investigate the stellar population physics of double-peaked emission-line galaxies, with the prospect of finding their commonality and individuality compared with a counterpart sample that comprises single-peaked emission-line galaxies.

The outline of this article is as follows. Section 2 features the selections and classifications of our sample, Section 3 describes the STARLIGHT software, Section 4 presents spectral synthesis results and analysis based on the sample, and a summary is given in Section 5.

## 2 SAMPLE SELECTION AND CLASSIFICATION

Our aim is to study the stellar population physics of double-peaked emission-line galaxies, which harbor unique nuclear activity, (i.e., dual AGNs) or disturbed NLRs related to outflows, inflows or disk rotation. In this work, the samples are selected from galaxies belonging to the LAMOST DR4 (Luo et al. 2015) and SDSS DR7 (Abazajian et al. 2009) data sets. Ge (2012) identified 3030 galaxies with double-peaked line profiles in prominent narrow emission lines, such as  $H\beta$ ,  $[O\ III]\lambda\lambda 4959, 5007$ ,  $H\alpha$  and  $[N\ II]\lambda\lambda 6548, 6584$  from SDSS DR7, while Dobos (2012) presented a comprehensive atlas of stacked spectra of galaxies with high signal-to-noise ratio (S/N) and resolution ( $S/N \simeq 132\text{--}4760$  at  $\Delta\lambda = 1\text{ \AA}$ ), which are classified by color, nuclear activity and star formation activity, from the same SDSS DR7 data set. The stacked spectrum atlas is available online<sup>1</sup>. Wang et al. (2019) built a sample of 325 objects displaying double-peaked narrow emission line features based on the LAMOST DR4 data set, while Wang et al. (2018) also provided a classification of typical emission-line galaxies based on the spectral line features of 40 182 galaxies from the LAMOST data products and created a set of stacked spectra<sup>2</sup> for diverse galaxy classes within LAMOST DR4.

To learn more about the features of double-peaked emission-line galaxies, we need a set acting as a reference sample manifesting single-peaked emission-line feature. Considering that the stacked spectra published in Dobos

(2012) and Wang et al. (2018) can represent the characteristics of typical emission-line galaxies and they are also drawn from the same sources (i.e., the SDSS DR7 and LAMOST DR4 databases), we consider them as the reference sample. Limited by current data samples, we are unable to construct a particularly detailed reference sample, such as a sample with the same stellar mass or similar redshift intervals. The ones defined in this work focus on Baldwin-Phillips-Terlevich (BPT) diagnosis (i.e., the emission-line flux ratio diagnostic diagram). As described in their works, according to the BPT diagnosis (Baldwin et al. 1981), the stacked spectra of galaxies published by Dobos (2012) and Wang et al. (2018) are classified into SF galaxies, composite galaxies (ones that fall into the transition region between SF and AGN, hereafter denoted by AGN + [H II] in order to distinguish them from composite spectra), Seyfert galaxies and low-ionization nuclear emission line regions (LINERs). Likewise, to get a general view of the stellar populations of double-peaked emission-line galaxies in different spectral classes and to improve the S/N of the spectra, we perform stellar population synthesis fittings on the so-called stacked spectra, which are combined from double-peaked emission-line galaxies from Ge (2012) and Wang et al. (2019), and can be seen as the representative spectra for different spectral classes. The spectral classes are divided based on the locations of each galaxy spectrum's blueshifted and redshifted components in the BPT diagram, and this will be described in more detail later in this section. We compare the stellar population synthesis results between the representative stacked spectra from double-peaked objects with their counterpart stacked typical emission-line spectra, both of which are classified based on different levels of activity, to give insight into the similarities and dissimilarities between the two.

As is well known, stellar population synthesis requires highly accurate continua of spectra. However, some uncertainties ( $<10\%$ ) are embedded in the shape of the continuum of LAMOST spectra (see Du et al. 2016), mainly due to its currently adopted method of relative flux calibration, which may bring about imprecise outputs of spectral fitting (Luo et al. 2015). The extinction uncertainties existing in standard stars (i.e., high-quality  $F$  dwarfs) may lead to errors in the deduced response curve and thus result in some uncertainty in flux calibration. Past analysis has also revealed that the lower the declination in which the object lies, the greater the uncertainty that would exist in its response curve (Wang et al. 2018). To obtain more accurate stellar populations, we adopt the method proposed in Wang et al. (2018) to eliminate the color inaccuracy in LAMOST spectra introduced by relative flux calibration. The method calibrates the original flux of each LAMOST

<sup>1</sup> <http://www.vo.elte.hu/compositeatlas>

<sup>2</sup> <http://sciwiki.lamost.org/downloads/w11>

spectrum using a low-order polynomial, which is derived from the fitting between LAMOST spectral flux and the converted flux constructed from the  $g$ ,  $r$  and  $i$  fiber magnitudes of its cross-referenced SDSS counterpart’s photometric catalog. As for the host redshift, which is of vital importance for line flux determination and stellar population analysis, we take it directly from the catalogs of Ge (2012) and Wang et al. (2019). The redshifts are derived from direct pixel-fitting of the stellar absorption lines with templates (i.e., the Indo-U.S. Library of Coudé Feed Stellar Spectra from Valdes et al. (2004)), and show a reasonable uncertainty of  $\sim 20 \text{ km s}^{-1}$ . Figure 1 presents the distribution of redshifts from the two samples. The redshifts of Ge’s samples are located between 0.0082 and 0.6352, with a median of 0.1379, while for samples from Wang et al. (2019), the redshifts range from 0.0271 to 0.3246, with a median value of 0.0968.

The stacked spectra of typical emission-line galaxies provided by Dobos (2012) and Wang et al. (2018) are representatives of SF galaxies, AGN + [H II], LINERs and Seyfert 2s based on the BPT diagram with classification lines suggested by Kewley et al. (2001) and Kauffmann et al. (2003). In Dobos (2012), the stacked spectra are constructed using a principal component analysis (PCA)-based method, while in Wang et al. (2018), the stacked spectra are developed by the median calculation. To make a one-to-one comparison, we also classify the double-peaked emission-line samples selected from SDSS and LAMOST in a similar way. Here we refer to the double-peaked emission-line profiles as multiple components composed of three kinematic groups, including the redshifted and blueshifted narrow emission lines ( $H\beta$ , [O III] $\lambda\lambda 4959, 5007$ ,  $H\alpha$  and [N II] $\lambda\lambda 6548, 6584$ ), the [O III] wings and broad Balmer emission lines. A Multi-Gaussian fitting is conducted to remodel each spectrum and the fluxes of the blueshifted and redshifted narrow components are derived from the fitting parameters. The blueshifted and redshifted narrow components can be created by different ionization mechanisms, and the nature of each component can be diagnosed by examining its location in the BPT diagram. Figure 2 shows the final samples in the BPT diagram, with the redshifted and blueshifted components being illustrated by different colors and symbols respectively. Dividing lines for the AGNs and SF galaxies developed by Kewley et al. (2001) and Kauffmann et al. (2003) are plotted as well. To distinguish Seyfert 2s from LINERs, an alternative dividing line from Cid Fernandes et al. (2010) is adopted, which proposes a more economical and simpler Seyfert/LINER division diagnosis than Kewley et al. (2006). As done in Ge’s catalog, the classification and statistical analysis are based

on the looser Kauffmann’s criteria, which take the galaxies that fall into the transition region as Type II AGNs. Here we reprocess and reclassify the spectra of 1945 narrow emission-line objects which are marked as ‘2 Type II’, ‘Type II+SF’ and ‘2 SF’ in his catalog. Finally we compose a new reclassification for 1473 objects from Ge’s catalog and 472 spectra are discarded owing to their high noise and non-ideal spectral multi-Gaussian fittings. For the catalog from Wang et al. (2019), since there are 18 Type I AGNs and 11 “unknown” type objects, as was stated in that work, we use the remaining 296 objects for analysis. As the blueshifted and redshifted components for each double peak could be driven by different mechanisms, several grouping combinations exist for the sample. In this work, the BPT types considered are SF galaxies, composite galaxies, Seyfert 2s and LINERs, and thus we refer to the 10 combined subgroups as types ‘2-SF’, ‘2-COM’, ‘2-Seyfert 2s’, ‘2-LINERs’, ‘SF+COM’, ‘SF+Seyfert 2s’, ‘SF+LINERs’, ‘Seyfert 2s+COM’, ‘COM+LINERs’ and ‘Seyfert 2s+LINERs’. Here, for instance, and hereafter, the type ‘2-SF’ stands for the combined subgroup in which each galaxy consists of two shifted SF components, while the Type ‘SF+Seyfert 2s’ corresponds to the subgroup in which each one consists of two shifted components falling into the SF and Seyfert 2s regions on the BPT diagram, respectively. Table 1 shows the number of spectra within each combined subgroup for 1473 objects from SDSS and 296 objects from LAMOST. In the end, we combine all spectra within each subgroup into one stacked spectrum by interpolating them uniformly and calculating the median intensity at each pixel as was done in Wang et al. (2018), and produce the 10 representative spectra for double-peaked emission-line galaxies from LAMOST and SDSS. Here, considering that the mean intensity calculated from each subgroup would be more vulnerable to poor spectra with high noise therein, we use the median method instead of a mean combination. As we can see, the combination of two shifted components could affect the continua, and thus the spectral energy distribution (SED) of double-peaked emission-line spectra will be different from that of their counterparts. Here we employ the software, called STARLIGHT (Cid Fernandes et al. 2005b)<sup>3</sup>, to fit the spectral absorption lines and continua of the stacked spectra and to obtain their stellar populations. In this way, we can quantify the uniqueness of these double-peaked emitting objects.

### 3 STELLAR POPULATION SYNTHESIS

STARLIGHT integrates the techniques initially developed for empirical population synthesis with the evolutionary

<sup>3</sup> <http://www.starlight.ufsc.br>

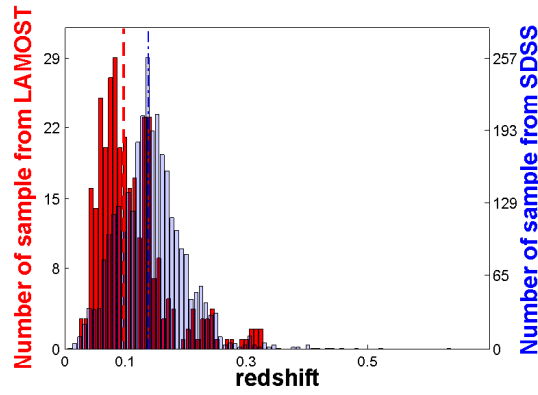


**Fig. 1** The *blue bars* signify the distribution of redshifts for 3030 samples from Ge (2012) selected from the SDSS DR7 database, and the *red bars* represent the distribution of redshifts for 325 samples from Wang et al. (2019) selected from the LAMOST DR4 database. The *blue dash-dotted line* and *red dashed line* stand for the median redshifts of samples from SDSS and LAMOST, respectively.

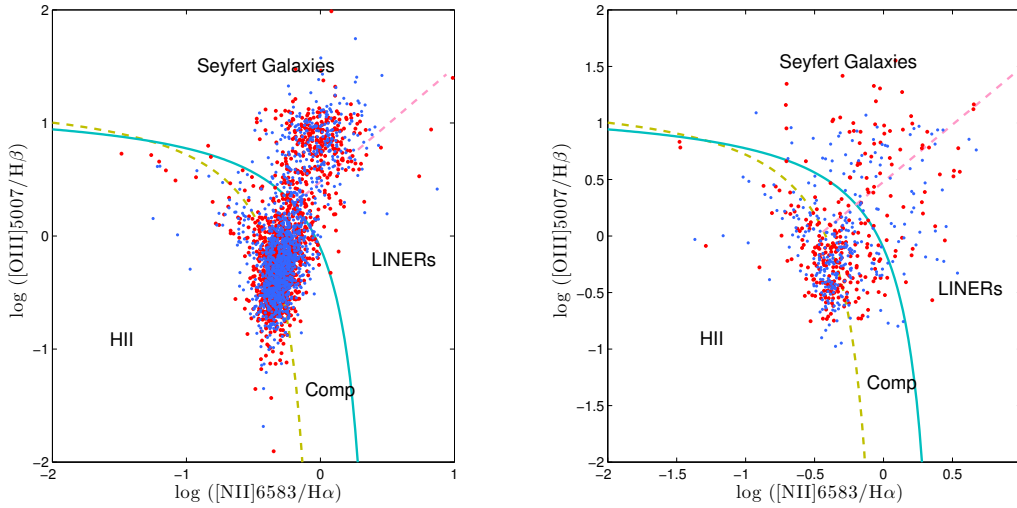


**Fig. 2** BPT diagrams of blue and red components of double-peaked emission-line samples from the SDSS DR7 database (*left panel*) and the LAMOST DR4 database (*right panel*). In both panels, the *green solid* and *yellow dotted lines* represent the classification lines suggested by Kewley et al. (2001) and Kauffmann et al. (2003), respectively, and the *pink dashed lines* signify the locus defined by Cid Fernandes et al. (2010) for Seyfert/LINER division. The *blue symbols* indicate the blueshifted component, and the *red symbols* correspond the redshifted component, for each selected target.

**Table 1** Number in Each Subsample

Combined BPT Subgroup	2-SF	2-COM	2-Seyfert 2s	2-LINERs	SF+COM	SF+Seyfert 2s	SF+LINERs	Seyfert 2s+COM	COM+LINERs	Seyfert 2s+LINERs
Sample from SDSS	305	478	208	12	302	7	3	59	43	56
Sample from LAMOST	96	48	28	10	60	2	8	11	15	18

**Table 2** Mid-values of Fractional Contributions in Three Representative Subgroups of SDSS from Ge (2012)

SSP		Emission-line Diagram			
		2-COM	SF+COM	SF+Seyfert 2s	SF+LINERs
Age	Young	25.3	30.9	27.0	16.4
	Intermediate	55.9	57.9	44.8	69.0
	Old	11.8	6.4	5.4	8.5
	Power law			11.2	5.3
$Z/Z_{\odot}$	0.2	51.4	55.5	61.1	14.9
	1.0	22.4	16.2	11.7	42.1
	2.5	18.7	18.5	6.2	27.1
	Power law			11.2	5.3

**Table 3** Quantified Stellar Populations of the Stacked Spectra of Double-peaked Emission-line Galaxies from the SDSS Sample Published in Ge (2012)

SSP		Subgroups from the Emission-line Diagram									
		2-SF	2-COM	2-Seyfert 2s	2-LINERs	SF+COM	SF+Seyfert 2s	SF+LINERs	Seyfert 2s+COM	COM+LINERs	Seyfert 2s+LINERs
Age	Young	35.0	28.4	7.5	7.4	32.5	27.3	14.8	6.5	13.7	6.5
	Intermediate	52.4	58.1	52.2	48.7	51.3	42.1	60.1	62.3	38.6	54.1
	Old	12.6	13.5	29.9	39.1	16.2	12.8	16.2	13.6	41.3	32.3
	Power law			10.4	4.8		17.8	8.9	17.6	6.4	7.1
$Z/Z_{\odot}$	0.2	55.2	44.3	16.6	3.7	50.5	63.4	39.4	23.7	38.1	9.8
	1.0	25.7	20.7	25.0	45.1	28.5	14.0	17.1	14.6	26.9	30.8
	2.5	19.1	35.0	48.0	46.4	21.0	4.8	34.6	44.1	28.6	52.3
	Power law			10.4	4.8		17.8	8.9	17.6	6.4	7.1

**Table 4** Quantified Stellar Populations of the Stacked Spectra of Double-peaked Emission-line Galaxies from the LAMOST Sample Published in Wang et al. (2019)

SSP		Subgroups from the Emission-line Diagram									
		2-SF	2-COM	2-Seyfert 2s	2-LINERs	SF+COM	SF+Seyfert 2s	SF+LINERs	Seyfert 2s+COM	COM+LINERs	Seyfert 2s+LINERs
Age	Young	51.7	32.4	15.4	14.5	53.8	43.3	48.5	18.2	38.1	22.1
	Intermediate	43.1	55.8	49.7	31.2	37.3	45.5	40.5	43.3	42.5	38.6
	old	5.2	11.8	34.1	52.7	8.9	5.8	11.0	28.4	15.6	36.5
	Power law			0.8	1.6		5.4	0.0	10.1	3.8	2.8
$Z/Z_{\odot}$	0.2	61.0	45.3	32.0	29.0	52.0	64.2	43.9	27.8	24.7	29.4
	1.0	32.5	21.7	24.1	39.0	36.9	15.4	43.3	32.1	24.1	24.7
	2.5	6.5	33.0	43.1	30.4	11.1	15.0	12.8	30.1	47.4	43.1
	Power law			0.8	1.6		5.4	0.0	10.1	3.8	2.8

synthesis models. Briefly speaking, an observed spectrum  $O_{\lambda}$  is fitted with a model  $M_{\lambda}$  that is a combination of  $N_{*}$  SSPs from the evolutionary synthesis models of BC03. The line-of-sight stellar motions are modeled by a Gaussian distribution  $G$ , with a central velocity  $v_{*}$  and a dispersion  $\sigma_{*}$ . Extinction is represented as the parameter  $V$ -band extinction  $A_v$ , and the Galactic extinction law from Cardelli, Clayton and Mathis (Cardelli et al. 1988) with  $R_v = 3.1$  being employed. In this work we use a base of 45 SSPs, including 15 ages ranging between 1 Myr and 13 Gyr and three levels of metallicities  $0.2 Z_{\odot}$ ,  $Z_{\odot}$  and  $2.5 Z_{\odot}$ . These spectra are extracted from the Stellar Library (STELIB, Le Borgne et al. (2003)), using the ‘‘Padova-2004’’ models and an IMF from Chabrier (2003). All these bases are normalized at a wavelength of  $4020 \text{ \AA}$ . Prior to STARLIGHT, at the pre-processing stage, we complete the foreground extinction correction using the reddening maps from Schlegel et al. (1998), bring all spectra to the rest frame based on the host redshifts and sample them into a step of  $1 \text{ \AA}$  from wavelengths  $3701 \text{ \AA}$  to  $8500 \text{ \AA}$ . Masked band regions for STARLIGHT input are also compiled (see Cid Fernandes et al. 2005b). The regions include the bands around bad pixels, emission lines, sky lines and some wavelength windows:  $5870\text{--}5905 \text{ \AA}$ , to skip the Na D  $\lambda\lambda 5890, 5896$  doublet;  $6845\text{--}6945 \text{ \AA}$  and  $7550\text{--}7725 \text{ \AA}$ . These ranges cover the bugs listed by BC03 resulting from problems in STELIB (Le Borgne et al. 2003);  $7165\text{--}7120 \text{ \AA}$ , which displays a systematic broad residual in emission as has been mentioned in Mateus et al. (2006) and  $5800\text{--}6100 \text{ \AA}$ , and is partly located in the

$200 \text{ \AA}$  overlapped range ( $5700\text{--}5900 \text{ \AA}$ ) between the red and blue band cameras of LAMOST. STARLIGHT directly provides the parameters of spectral synthesis; one important parameter is the population vector  $x_j$  ( $j = 1, \dots, N_{*}$ ), which reveals the contribution of each SSP to model flux at the normalized wavelength  $4020 \text{ \AA}$ .

## 4 SYNTHESIS RESULTS

### 4.1 Detailed Description of the Synthesis Results

We take the combined subgroups ‘2-COM’, ‘SF+COM’, ‘SF+Seyfert 2s’ and ‘SF+LINERs’ from the SDSS sample as an example, to assess the reliability of stacked spectra as the representative ones for stellar population analysis in this work. The subgroup ‘2-COM’ is selected since it harbors the largest sample within these combined subgroups, as we can see from Table 1 and each galaxy within it has the same BPT diagnosis for its blueshifted and redshifted emission-line components. The subgroup ‘SF+COM’ is chosen to stand for types whose dual shifted components exhibit different BPT classifications. The subgroups ‘SF+Seyfert 2s’ and ‘SF+LINERs’ are also selected, as these two include only seven and three objects respectively, and with these we can assess the robustness of stacked spectra in sparse samples. We perform stellar population synthesis on all spectra from the four representative subgroups and get the fractional contributions of populations, within three different bins of age and three levels of stellar metallicity, to produce a light profile for each galaxy spectrum (these six types of quantified stel-

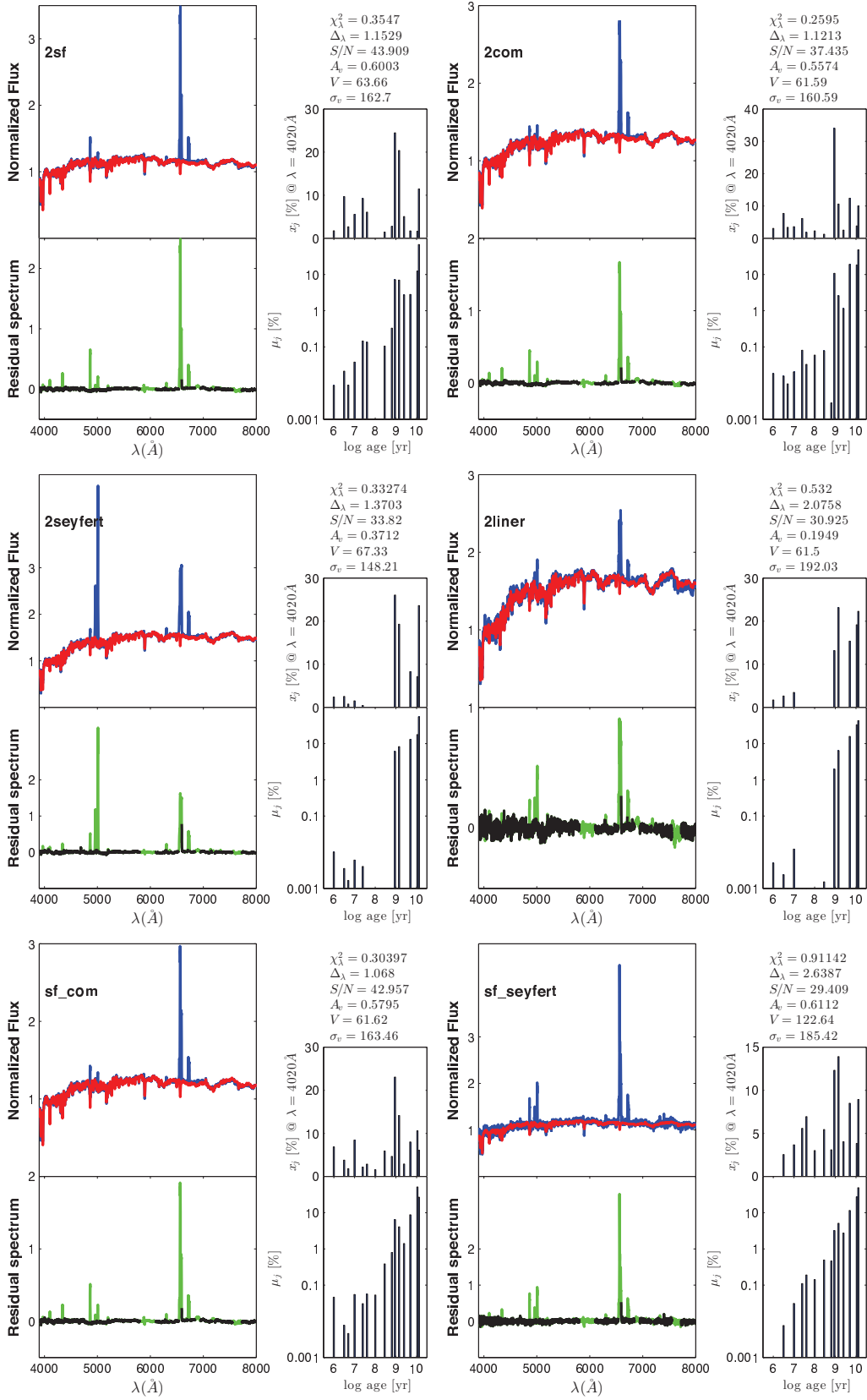


**Fig. 3** Spectral synthesis outputs of six stacked spectra for double-peaked emission-line galaxies from the SDSS sample published in Ge (2012). Each sub-figure shares the same layout as Fig. A.1, and the types of the six stacked spectra are also tagged in the top left of each sub-figure. All symbols are the same as in Fig. A.1.

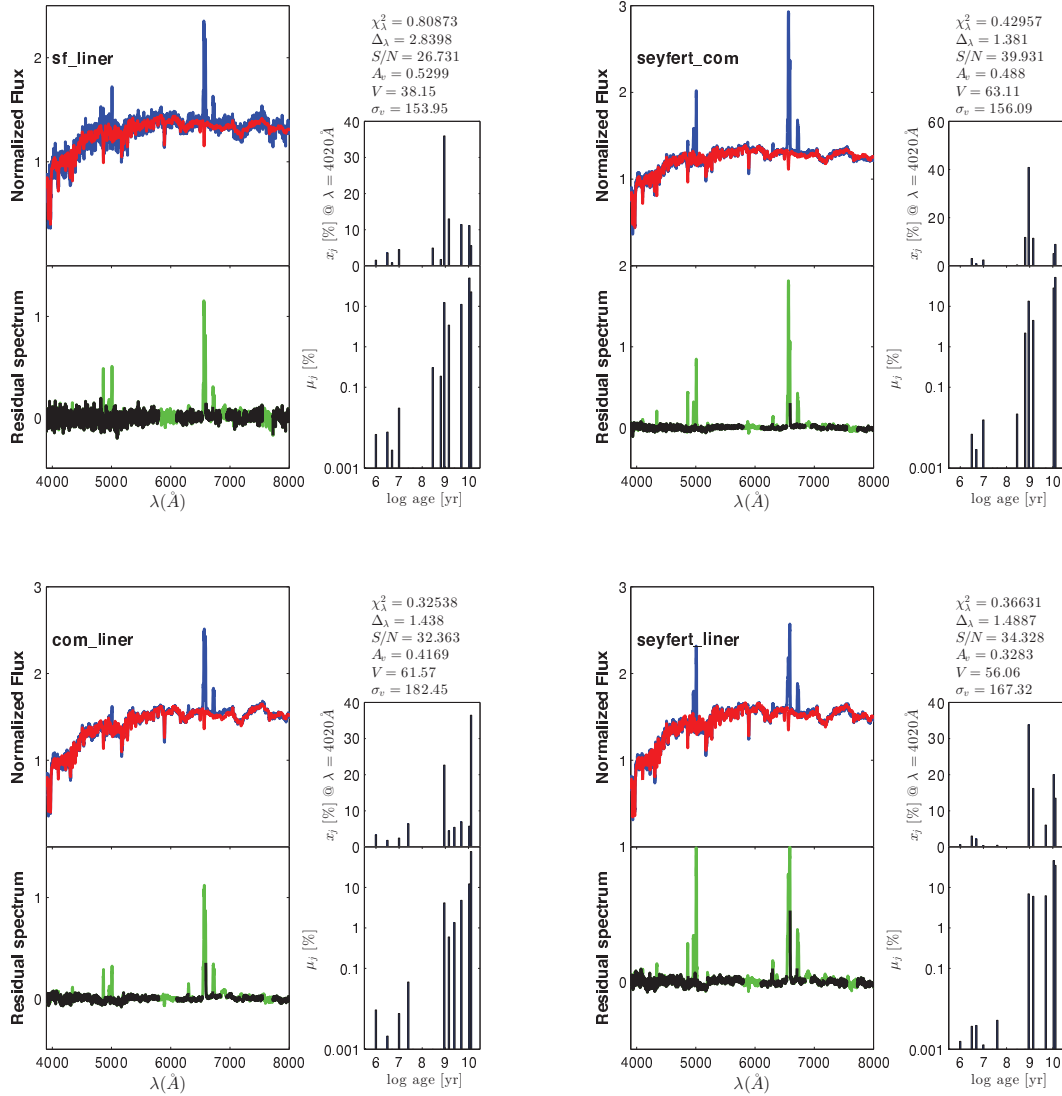


**Fig. 4** Spectral synthesis outputs of the remaining four stacked spectra for double-peaked emission-line galaxies from the SDSS sample published in Ge (2012). Each sub-figure shares the same layout as Fig. A.1, and the types of the four stacked spectra are also tagged in the top left of each sub-figure. All symbols are the same as in Fig. A.1.

lar populations will be described in detail in Sect. 4.2). Then we calculate the mid-values of the contributing percentages for each subgroup, and list the results in Table 2. We compare the results with the counterpart values in Table 3, which presents the percentages of light contributions to 10 stacked spectra constructed from different combined subgroups. We can see that for subgroups ‘2-COM’, ‘SF+COM’ and ‘SF+Seyfert 2s’, the synthesis results displayed in Tables 2 and 3 manifest similar proportional distributions. As for subgroup ‘SF+LINERS’, in which there are only three spectra, it still shows a similar proportional distribution between results deduced from the stacked spectrum and all involved spectra, when we focus on the contributions from populations with different ages. However, this is not the case when we consider the

contributions from populations of different stellar metallicities. As we can see, it is never an easy task to generate an ideal stacked spectrum from such a small sample size, since in this case the representative spectrum would be more susceptible to some spectrum with poor spectral quality when being constructed. As posed above, and considering that the subgroup ‘SF+Seyfert 2s’ includes only seven samples but still produces a reliable stacked spectrum, we can conclude that the stacked spectrum can reflect the commonalities of samples within its subgroup in most cases. In the following analysis, for some subgroups (i.e., SF+Seyfert 2s from LAMOST, SF+LINERS from SDSS, see Table 1), which contain fewer than seven objects, we take the result as a reference.

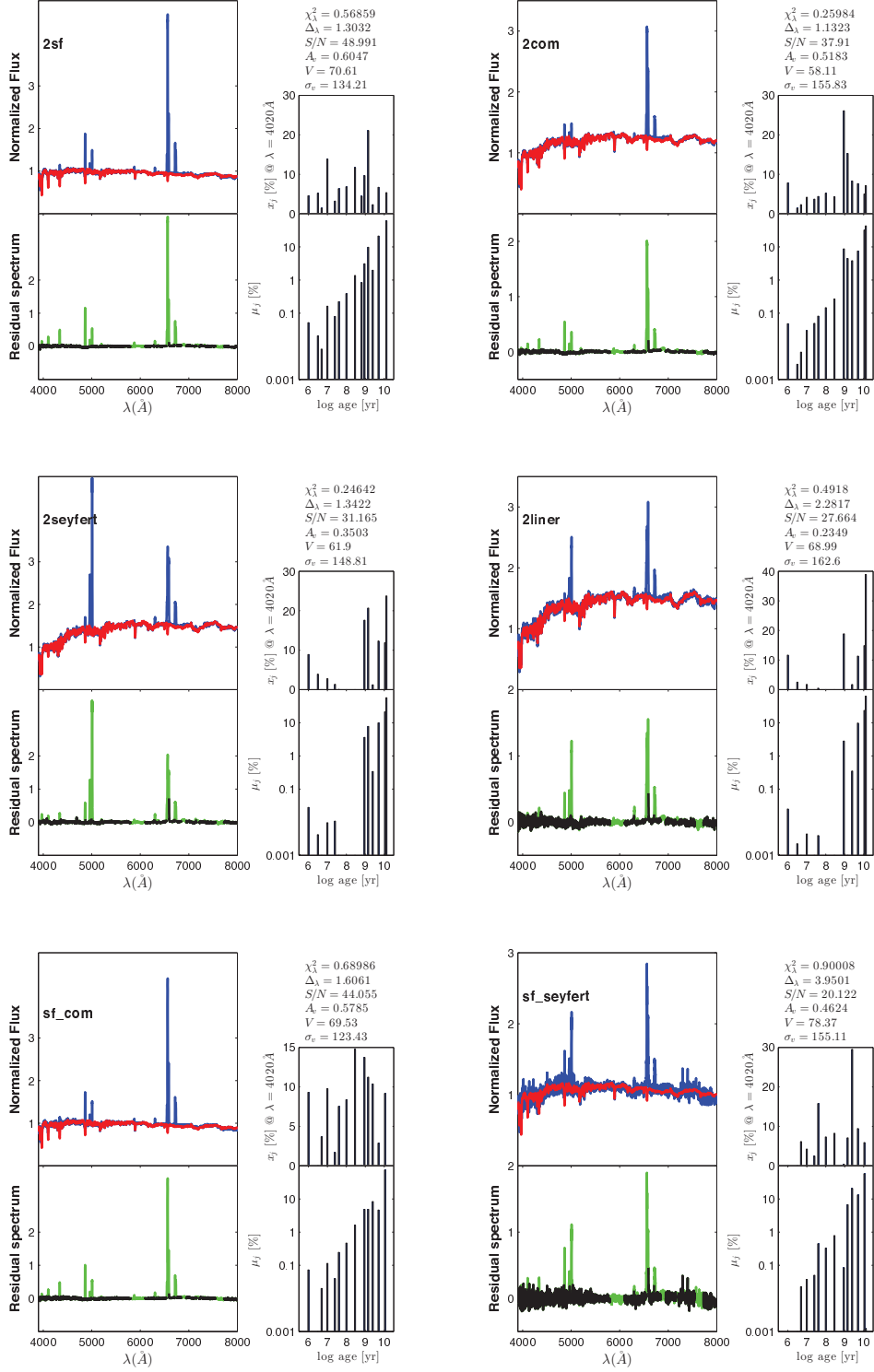


**Fig. 5** Spectral synthesis outputs of six stacked spectra for double-peaked emission-line galaxies from the LAMOST sample published in Wang et al. (2019). Each sub-figure shares the same layout as Fig. A.1, and the types of the six stacked spectra are also tagged in the top left of each sub-figure. All symbols are the same as in Fig. A.1.

#### 4.2 Results and Comparisons Based on the SDSS Data Set

At first, we apply STARLIGHT to the stacked spectra from the SDSS sample published in Dobos (2012). Figures A.1

to A.4 in Appendix A show the synthesis outputs (the layout of each figure and its supplementary information will be explained in Appendix A). In this analysis, we use a coarse but robust description of the star formation history

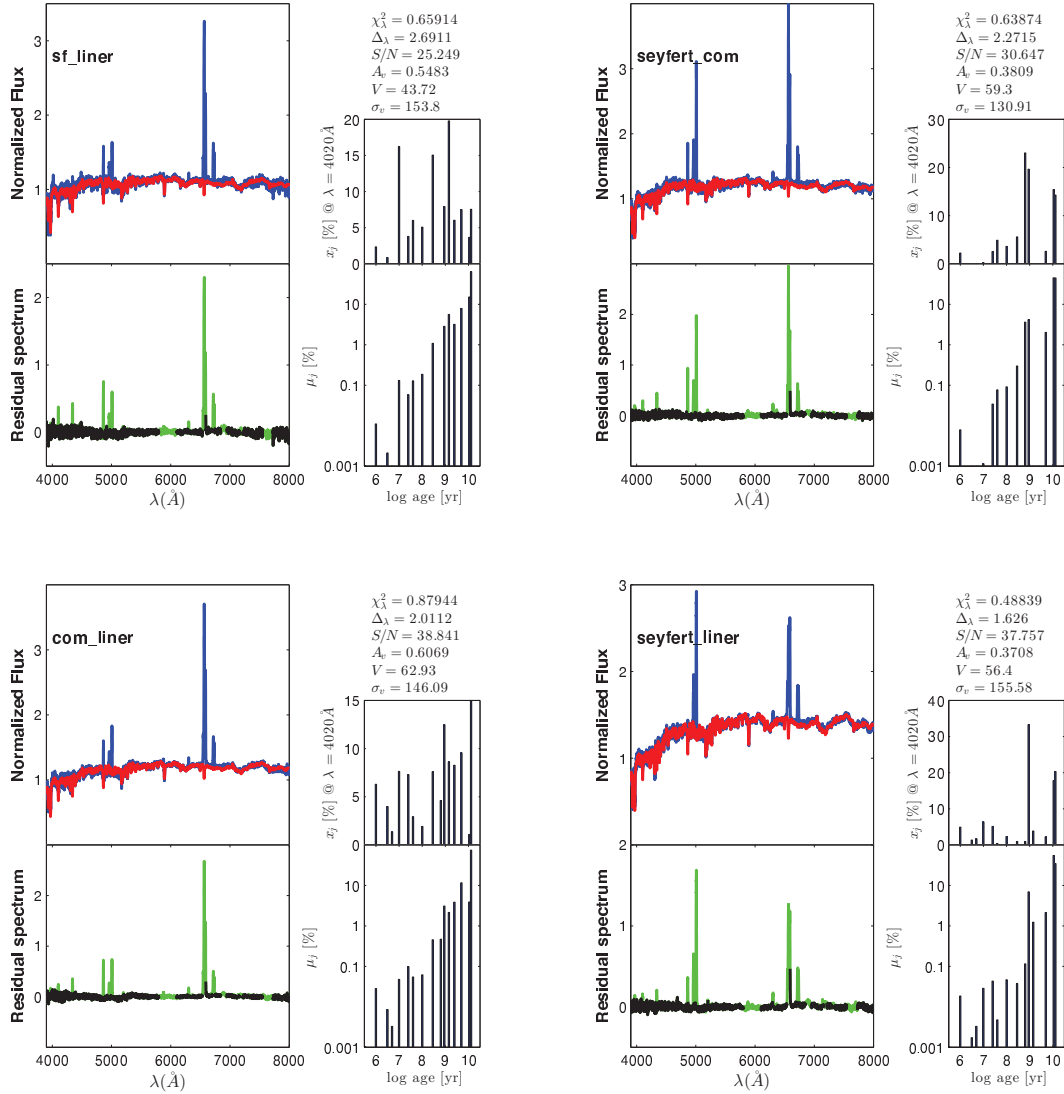


**Fig. 6** Spectral synthesis outputs of the remaining four stacked spectra for double-peaked emission-line galaxies from the LAMOST sample published in Wang et al. (2019). Each sub-figure shares the same layout as Fig. A.1, and the types of the four stacked spectra are also tagged in the top left of each sub-figure. All symbols are the same as in Fig. A.1.

of a galaxy by dividing the ages of stellar populations into three bins: ‘young’ ( $\leq 5 \times 10^8$  yr), ‘intermediate-age’ ( $6.4 \times 10^8$  yr  $\leq$  age  $\leq 5 \times 10^9$  yr) and ‘old’ ( $\geq 1 \times 10^{10}$  yr), with the same criteria adopted in Cid Fernandes et al. (2005b). Table A.1 presents the fractional contributions of populations within the three quantified age bins and three levels of stellar metallicity to the model flux, respectively. From Table A.1, we can see that SF galaxies, AGN + [H II] and Seyfert 2s hold abundant young and intermediate-age populations (from 92.3% to 74.3%), while LINERs contain a great deal of intermediate-age and old populations ( $\sim 86\%$ ). There also exists an obvious decrease in young population contribution from SF galaxies, AGN + [H II] and Seyfert 2s to LINERs, which is consistent with the conclusion in previous articles (e.g., Boisson et al. 2004;

Chen et al. 2009; Stasińska et al. 2008), since the activities in Seyfert 2s and LINERs are perceived to be linked to nuclear, or possibly shocks for LINERs, while those in SF galaxies are dominated by stellar activities of young stars. Another conclusion we can draw from Figures A.1 to A.4 is that the intermediate-age and old populations contribute the vast majority of mass in all these subsamples, which also agrees with the phenomena observed by Chen et al. (2009). As for the analysis of metallicity contributions, since we are considering three levels of metallicity,  $0.2 Z_\odot$ ,  $Z_\odot$  and  $2.5 Z_\odot$ , we calculate the percentages by adding up the contributions of relevant SSPs within each metallicity grid. It can be seen from Table A.1 that SF galaxies and AGN + [H II] are dominated by metal-poor populations with metallicity  $0.2 Z_\odot$ , while Seyfert 2s

and LINERs possess a large contribution from a population with metallicity  $Z_{\odot}$ . We can see from Table A.1 that LINERs are dominated by populations with metallicity  $Z_{\odot}$  and ‘old’ age, while there is little contribution from populations with metallicity  $0.2Z_{\odot}$  and ‘young’ age, which indicate their features of oldest, evolved metal-rich and little star formation activity, as was summarized in Boisson et al. (2004). A power law, which represents the non-stellar component (Koski 1978), is also added for the spectral fitting of LINERs and Seyfert 2s. The flux contributions of the power-law spectrum in Seyfert 2s and LINERs are both small, at less than  $\sim 1\%$ , which is different from what has been concluded in past works and in synthesis outputs on other stacked spectra in this work. This irrational output may be attributed to the PCA-based method used by Dobos (2012) when computing the average spectra, which is different from the traditional averaging and median calculation applied by us. The PCA-based method may ignore this featureless continuum component, and this needs to be further verified.

For the double-peaked emission line samples from the SDSS DR7 database published in Ge (2012), and as discussed in Section 2, these galaxies are divided into 10 sub-categories according to the locations of their blueshifted and redshifted components on the BPT diagram. To better illustrate the commonality and properties of each subsample, we combine all spectra within each subgroup into one stacked spectrum. Figures 3 and 4 display the synthesis outputs for each stacked spectrum of 10 subgroups from STARLIGHT, by employing 45 SSPs from BC03, with each sub-figure sharing the same layout and interpretation as Figure A.1. Table 3 also lists the calculated contributions of different types of stellar populations within each subgroup. Since the population synthesis outputs from Dobos’ spectra can represent the regular properties of galaxies from the SDSS DR7 database, we analyze their similarities and differences, to learn more about the properties of double-peaked emission-line galaxies. In Table 3, columns 3 to 6 list the synthesis results for double-peaked emission-line objects holding two shifted components with the same BPT diagnosis; we compare the results with the counterpart ones listed in Table A.1. As for the contributions from stars with different ages, we can see that there still exists a trend in terms of the decrease of significance for the young population from 2-SF, 2-COM, 2-Seyfert 2s to 2-LINERs with 2-LINERs holding the largest ‘old’ population contribution, having a similar distribution as displayed in Dobos’ stacked spectra. Besides these, we also notice some differences. The predominant population of ages in the single-peaked SF galaxy spectrum is the young population, while in the stacked 2-SF spec-

trum, it turns out to be the intermediate-age population, with a marked percentage of  $\sim 52\%$ . Although displaying a similar trend, the contribution from the young population for each subgroup in Ge’s sample is less obvious than in its counterpart in Dobos’ results. For the stacked spectrum of all 2-Seyfert 2s, which are the most probable dual AGN candidates, the fractional contributions from intermediate-age and old populations increase significantly to a total of  $\sim 82\%$ , revealing more vividly nuclear activities in this kind of sample. Considering the metallicity effects, the dominant contribution remains unchanged within subgroups 2-SF and 2-COM, while in subgroups 2-Seyfert 2s and 2-LINERs, the main contributions come from populations with metallicity  $2.5Z_{\odot}$ . Then, we analyze results from spectra hosting components of different BPT types. Although the analysis would be susceptible to the influence of various proportions of different components, we still notice an apparent trend. The sample which integrates one component of SF galaxy type is obviously rich in young and intermediate-age populations (from  $\sim 69.4\%$  to  $\sim 83.8\%$ ), and the sample which holds one component of LINER type (except for the SF+LINERs subgroup), hosts impressive contributions from old populations (from  $\sim 32.3\%$  to  $\sim 41.3\%$ ), with an obviously larger value than in other combined subgroups. The contribution of young populations in each combined subgroup appears to be obviously less than its counterpart in Dobos’ stacked spectra, indicating that the double-peaked emitting phenomenon is more likely to happen in an ‘older’ stellar environment. We also find that the subgroups with different BPT types (except for Seyfert 2s+LINERs) show a significant contribution from populations with metallicities  $0.2$  and  $2.5Z_{\odot}$ , which suggests that the star formation history of these double-peaked emission-line samples is remarkably heterogeneous: young starbursts and old stellar populations all appear in significant and widely varying proportions. For all subgroups that contain one Seyfert II or LINER component, a power-law is considered when carrying out the fittings, and the contributions of this featureless continuum component in different subgroups range from  $\sim 4.8\%$  to  $\sim 17.8\%$ .

### 4.3 Results and Comparisons Based on the LAMOST Data Set

We also employ STARLIGHT on stacked spectra generated by Wang et al. (2018) and Wang et al. (2019) from the LAMOST database, still using 45 SSPs with the 15 representative ages and three metallicities as mentioned in Section 4.2. In Appendix A, Figures A.5 to A.8 illustrate the spectral fits obtained for the stacked spectra provided by Wang et al. (2018) drawn from the LAMOST

DR4 database, and Table A.2 lists the normalized fractional contributions of SSPs with three bins of age and three grids of metallicity for four stacked spectra from Wang et al. (2018), calculated from STARLIGHT output parameter  $x_j$ . As we can see from this table, the synthesis outputs display approximately the same contribution trend in terms of stellar populations as in Dobos’ stacked spectra. Except that in view of the metallicity effect, the dominant contributions to SF galaxies and AGN + [H II] come from populations with metallicity  $Z_{\odot}$ , while it appears to be  $0.2 Z_{\odot}$  in Dobos’ results. Figures 5 and 6 display the synthesis outputs for 10 stacked spectra constructed from double-peaked emission-line galaxies in LAMOST DR4, and Table 4 lists the percentages for light fractions given by the synthesis outputs. We still notice the decrease in significance of the young population in types 2-SF, 2-COM, 2-Seyfert 2s to 2-LINERs, which has been shown in stacked spectra from Ge (2012). We compare the percentages with the counterpart values listed in Table A.2. The significances of young populations in 2-SF, 2-COM and 2-Seyfert 2s are relatively lower, with an average percentage of  $\sim 7.5\%$ . We can see that this phenomenon is consistent with the conclusion drawn from the similar comparison between Ge’s and Dobos’ synthesis results in Section 4.2. Regarding stacked spectra holding different BPT components, the subgroups consisting of an SF component are obviously rich in young and intermediate-age populations, with the percentages ranging from 88.8% to 91.1%, while the ones consisting of Seyfert 2s or LINERs component would be abundant in intermediate-age and old populations, with the percentages ranging from 58.1% to 71.7%. Here the contributions of a power-law component to different subgroups range from  $\sim 0.8\%$  to  $\sim 10.1\%$ .

## 5 SUMMARY

This study focuses on the stellar population physics of double-peaked emission-line galaxies, which have long been perceived as objects related to merging galaxies or other phenomena of disturbed dynamical activities in NLRs. We group and stack spectra of the double-peaked emitting galaxies published in Ge (2012) and Wang et al. (2019), which are selected from the SDSS DR7 and LAMOST DR4 databases, respectively. In this work, we fit each double-peaked emission-line sample with multi-Gaussian profiles and classify them according to the BPT types of the blueshifted and redshifted components. For each class, the spectra have the same assembled pair of BPT type components. Then, we stack spectra of each class for further study. We also choose the stacked single-peaked emission-line galaxies published in Dobos (2012) and Wang et al. (2018) as the control sample. The single-

peaked spectra are also picked out from the SDSS DR7 and LAMOST DR4 databases and categorized based on BPT types. We fit the continua and spectral absorptions of stacked spectra by using STARLIGHT and 45 SSPs from BC03, and then compare the synthesis results of double-peaked emission-line samples with those of single-picked counterparts, from the SDSS and LAMOST databases, independently. From the analysis of emitted light, we find that the significance of young populations shows a downward trend from 2-SF, 2-COM and 2-Seyfert 2s to 2-LINERs, which is similar to the corresponding reference sample. However, the contribution of young populations to the light of stacked spectra with double-peaks is less than that of single-peaked spectra, which reveals that the double-peaked emitting phenomenon is more likely to happen in an ‘older’ stellar environment. The subgroups consisting of an SF component are obviously rich in young and intermediate-age populations in most cases, while the ones consisting of a Seyfert 2 or LINER component tend to be abundant in intermediate-age and old populations, confirming the strong correlations between stellar populations and their spectral classes. Concerning the metallicity effects, subgroups 2-SF and 2-COM are metal-poor, while for subgroups 2-Seyfert 2s and 2-LINERs, the main contributions come from populations with metallicities of  $Z_{\odot}$  and  $2.5 Z_{\odot}$ . The subgroups with different BPT types usually, although not absolutely, show a significant contribution from populations with metallicities of 0.2 and  $2.5 Z_{\odot}$ , presenting a heterogeneous feature. This feature suggests a more complicated star formation history encoded in these double-peaked emission-line samples than in the corresponding single-peaked emission-line samples.

**Acknowledgements** This work was funded by the National Natural Science Foundation of China (NSFC) (Grant No. 11603042) and the China Scholarship Council. The STARLIGHT project is supported by the Brazilian agencies CNPq, CAPES and FAPESP, and by the France-Brazil CAPES/Cofecub program. We thank the wonderful database from the LAMOST and SDSS surveys. We thank Ge (2012), Dobos (2012) and Wang et al. (2018) for their great job.

## Appendix A: SPECTRAL SYNTHESIS FITTINGS OF THE CONTROL SAMPLES

Figures A.1 to A.4 show the synthesis outputs of the stacked spectra for different types of galaxies within the SDSS sample from Dobos (2012). In each figure, the top-left panel displays the stacked spectra (blue line) and the synthesis model (red line), the bottom-left one shows the residual (i.e., the pure emission line spectrum), which is

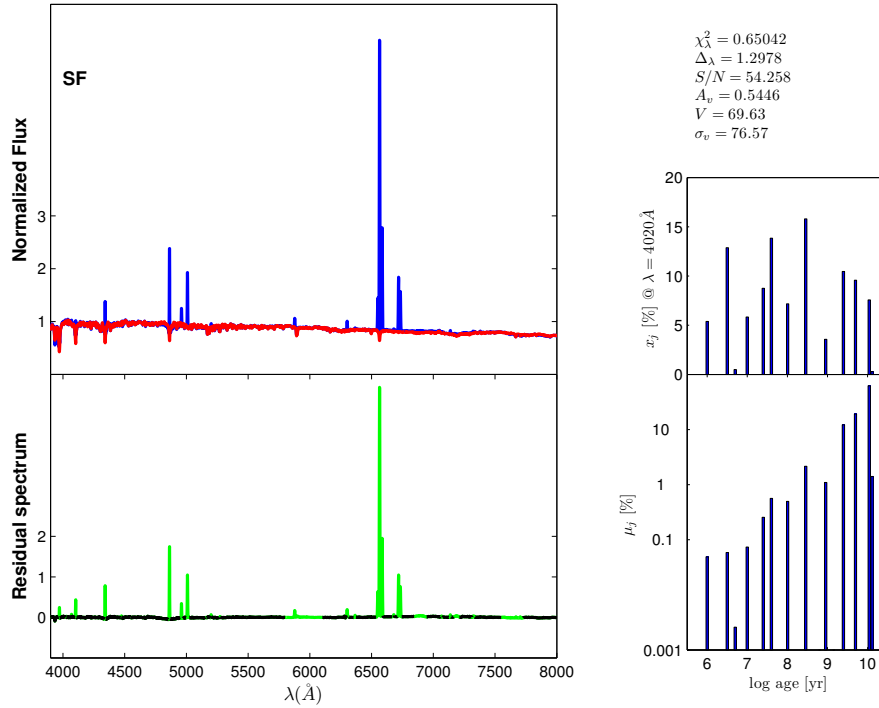


**Fig. A.1** Spectral synthesis outputs of the stacked spectrum for SF galaxies within the SDSS sample from Dobos (2012). The layout of this figure is as below. Top left: stacked spectrum (blue line), synthesis spectrum (red line). Bottom left: residual spectrum (black line), masked regions (green line). Right: fractions of flux (top) and mass (bottom) as a function of age, in the logarithmic coordinate. In the top right, some deduced parameters are listed, which have been explained in the text.

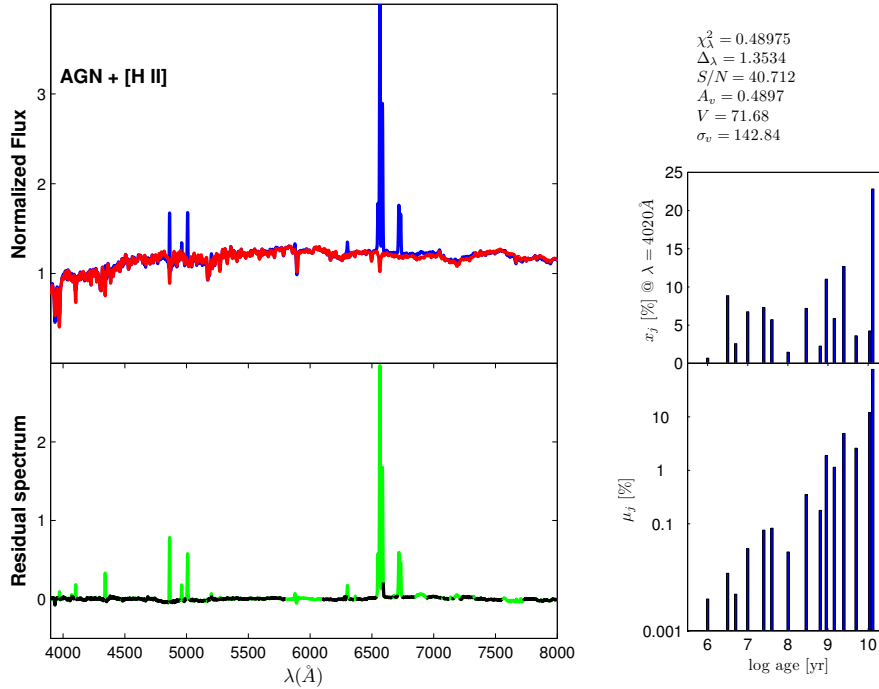


**Fig. A.2** Spectral synthesis outputs of the stacked spectrum for AGN + [H II] galaxies within the SDSS sample from Dobos (2012). This figure shares the same layout and symbols as Fig. A.1.

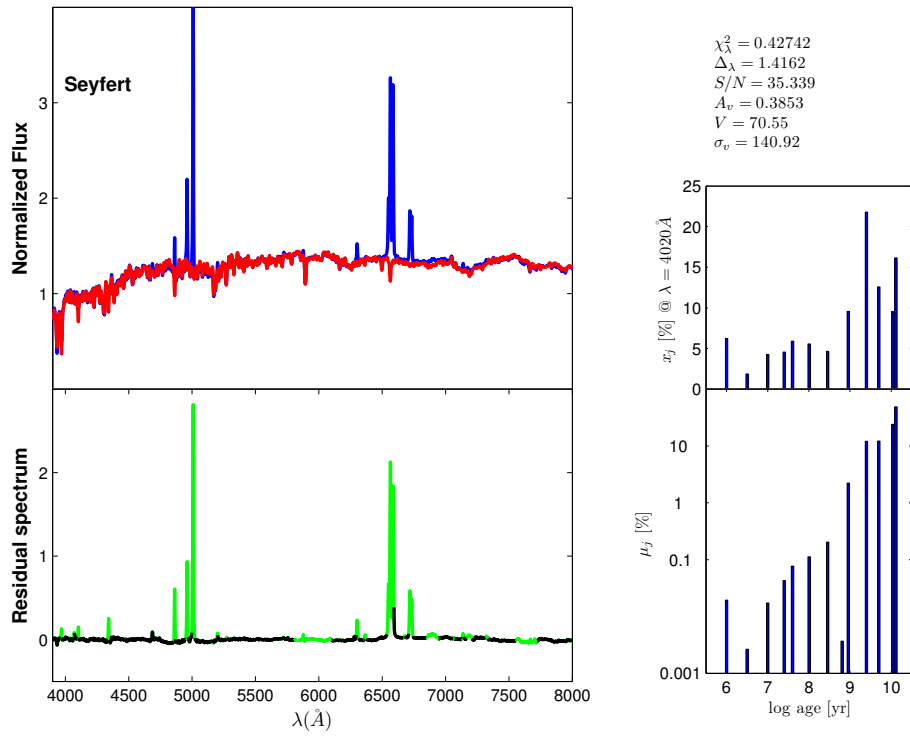


**Fig. A.3** Spectral synthesis outputs of the stacked spectrum for Seyfert 2s within the SDSS sample from Dobos (2012). This figure shares the same layout and symbols as Fig. A.1.

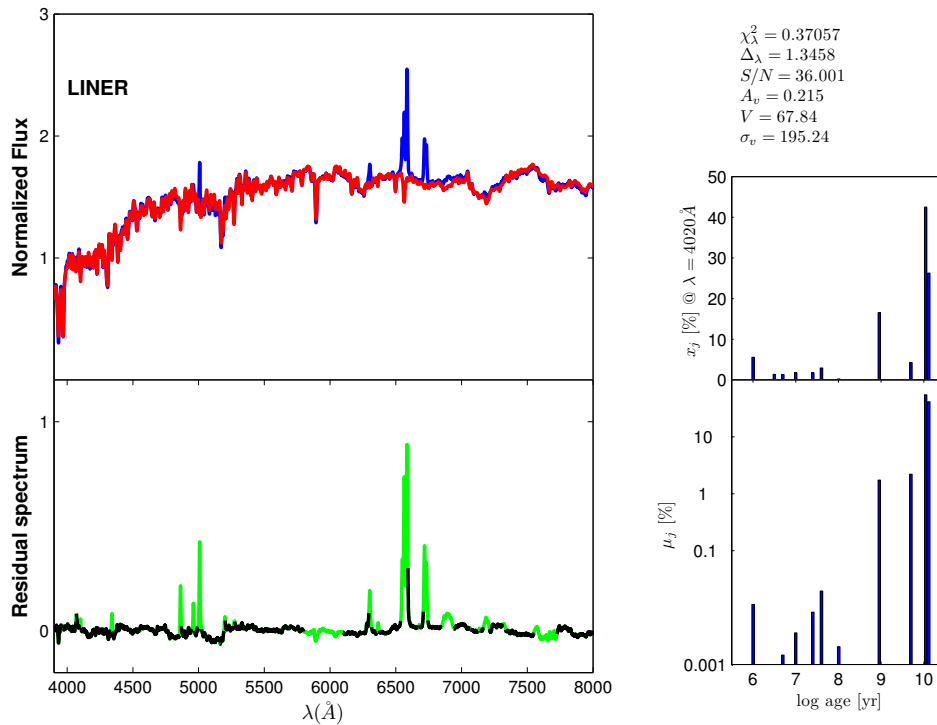


**Fig. A.4** Spectral synthesis outputs of the stacked spectrum for LINERs within the SDSS sample from Dobos (2012). This figure shares the same layout and symbols as Fig. A.1.

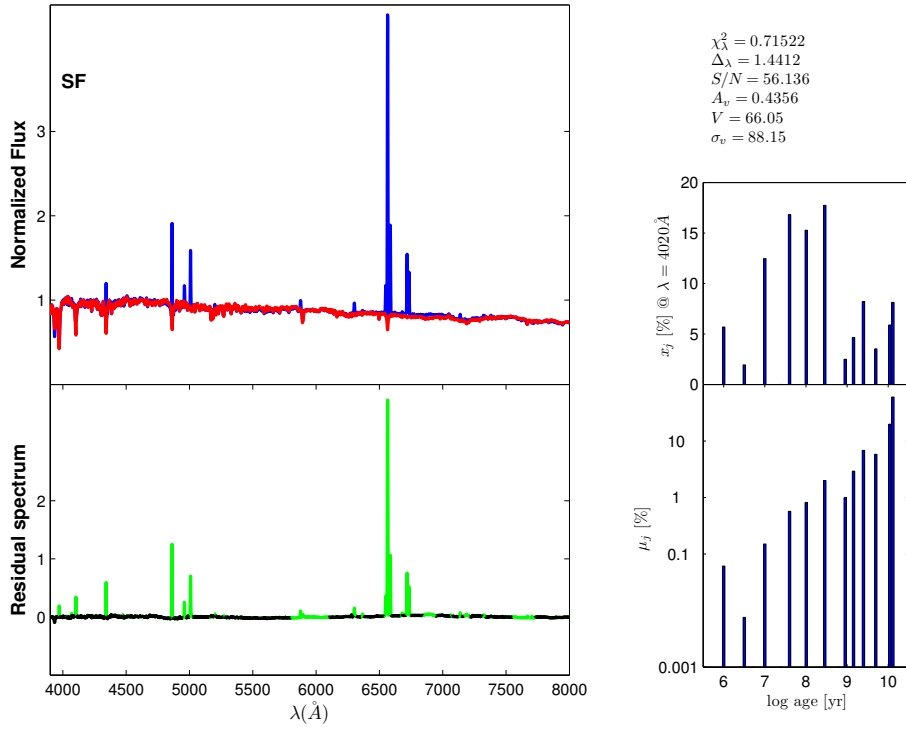


**Fig. A.5** Spectral synthesis outputs of the stacked spectrum for SF galaxies within the LAMOST sample from Wang et al. (2018). This figure shares the same layout and symbols as Fig. A.1.

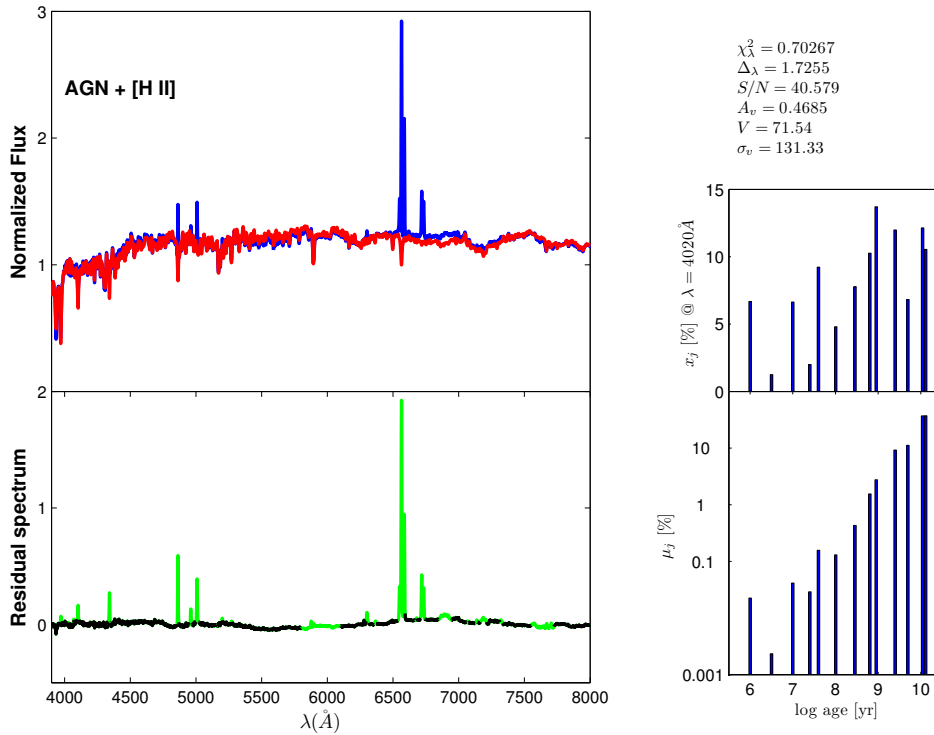


**Fig. A.6** Spectral synthesis outputs of the stacked spectrum for AGN + [H II] galaxies within the LAMOST sample from Wang et al. (2018). This figure shares the same layout and symbols as Fig. A.1.

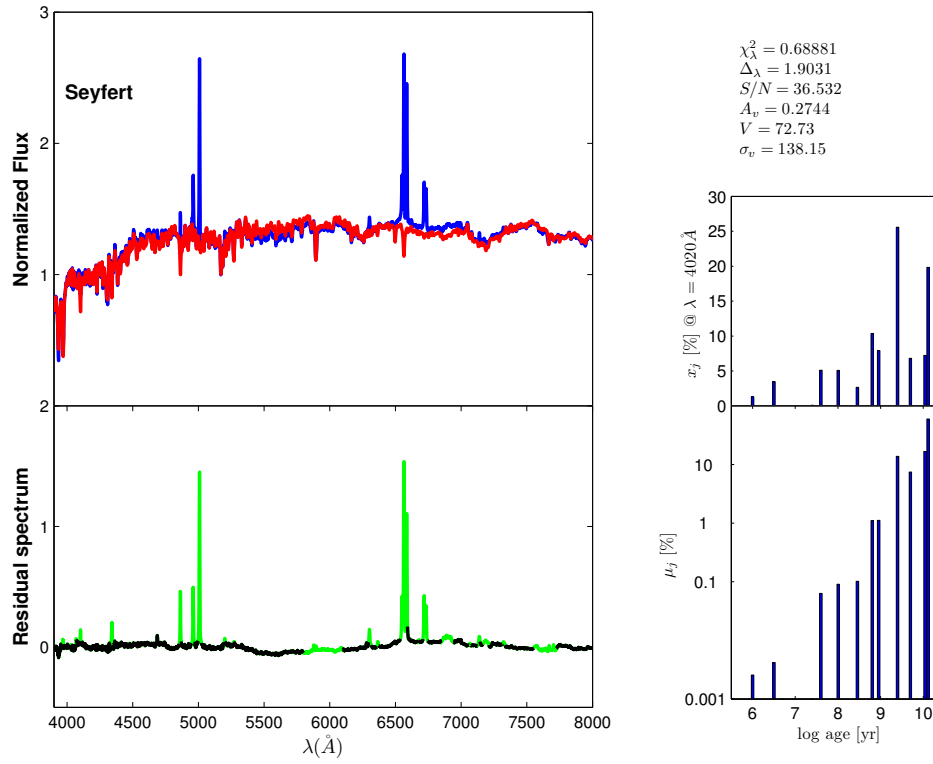


**Fig. A.7** Spectral synthesis outputs of the stacked spectrum for Seyfert 2s within the LAMOST sample from Wang et al. (2018). This figure shares the same layout and symbols as Fig. A.1.

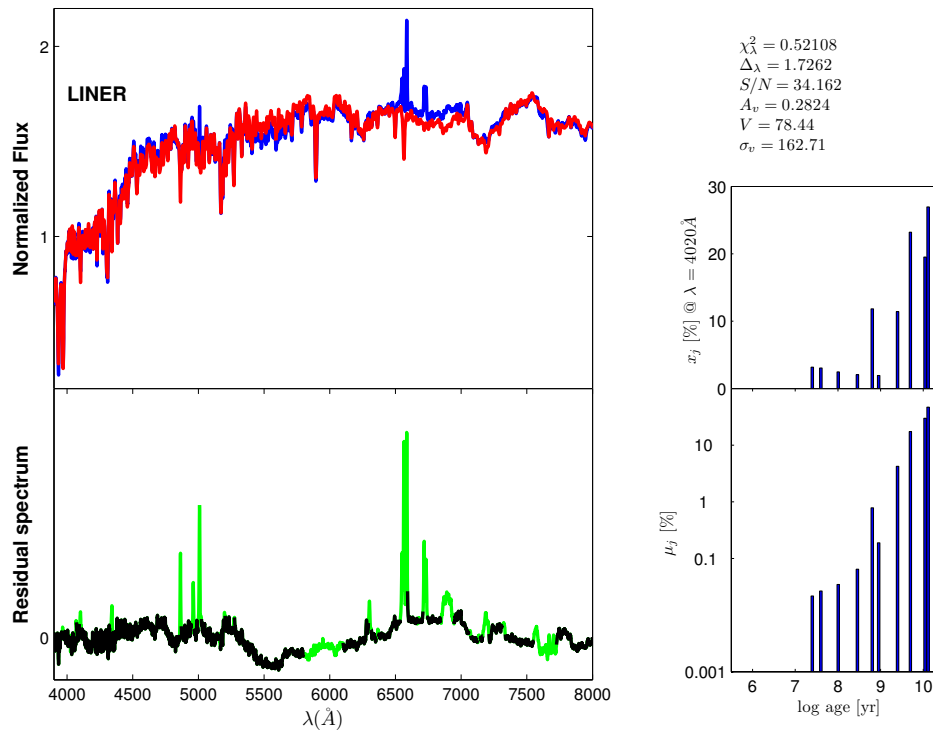


**Fig. A.8** Spectral synthesis outputs of the stacked spectrum for LINERs within the LAMOST sample from Wang et al. (2018). This figure shares the same layout and symbols as Fig. A.1.

**Table A.1** Quantified Stellar Populations of the Stacked Spectra from the SDSS Sample Published in Dobos (2012)

SSP		Emission-line Diagram			
		SF galaxies	AGN + [H II]	Seyfert 2s	LINERs
Age	Young	69.1	39.3	31.5	13.9
	Intermediate	23.2	34.4	42.8	19.9
	Old	7.7	26.3	25.0	65.9
	Power law			0.7	0.3
$Z/Z_{\odot}$	0.2	55.3	47.8	27.1	17.8
	1.0	44.0	41.4	63.5	66.4
	2.5	0.7	10.8	8.7	15.5
	Power law			0.7	0.3

**Table A.2** Quantified Stellar Populations of the Stacked Spectra from the LAMOST Sample Published in Wang et al. (2018)

SSP		Emission-line Diagram			
		SF galaxies	AGN + [H II]	Seyfert 2s	LINERs
Age	Young	68.0	37.0	17.0	10.2
	Intermediate	18.4	41.2	48.8	43.7
	Old	13.6	21.8	26.1	44.0
	Power law			8.2	2.1
$Z/Z_{\odot}$	0.2	39.5	19.6	8.1	5.9
	1.0	60.5	71.2	70.1	83.2
	2.5	0.0	9.2	13.6	8.8
	Power law			8.2	2.1

plotted with a black line, and the masked regions, which are plotted with a green line, while the two right panels illustrate the deduced star formation history embedded in the population vectors  $x_j$  and  $u_j$ , which are both age-binned in the logarithmic coordinate.  $x_j$  reveals the contribution of each SSP to the model flux at the normalized wavelength  $4020 \text{ \AA}$ , while  $\mu_j$  represents the mass fraction vector. As supplementary information, some derived properties are also listed in the top right. Here are the reduced  $\chi^2$ ;  $\Delta_{\lambda}$ , revealing the difference between the observed spectra and the synthesis model; S/N, which is obtained in a specified region around  $4020 \text{ \AA}$ ;  $A_v$  is referred to as the  $V$ -band extinction; the kinematic parameters, velocity  $v$  and velocity dispersion  $\sigma_v$ . Table A.1 presents the fractional contributions of populations within three quantified age bins and three levels of stellar metallicity to the model flux.

Figures A.5 to A.8 illustrate the spectral fits obtained for the stacked spectra provided by Wang et al. (2018) drawn from the LAMOST DR4 database, which can serve as a reference sample to enable us to learn more about the unique characteristics of double-peaked emission-line galaxies. Each figure shares the same layout and symbols as Figure A.1. Table A.2 lists the normalized fractional contributions of SSPs with three bins of age and three grids of metallicity for four stacked spectra from Wang et al. (2018), calculated from STARLIGHT output parameter  $x_j$ .

## References

Abazajian, K. N., Adelman-McCarthy, J. K., Agüeros, M. A., et al. 2009, *ApJS*, 182, 543

- Bacon, R., Brinchmann, J., Richard, J., et al. 2015, *A&A*, 575, A75
- Baldwin, J. A., Phillips, M. M., & Terlevich, R. 1981, *PASP*, 93, 5
- Barrera-Ballesteros, J. K., Sánchez, S. F., García-Lorenzo, B., et al. 2015, *A&A*, 579, A45
- Blecha, L., Loeb, A., & Narayan, R. 2013, *MNRAS*, 429, 2594
- Boisson, C., Joly, M., Pelat, D., & Ward, M. J. 2004, *A&A*, 428, 373
- Bressan, A., Chiosi, C., & Tantalò, R. 1996, *A&A*, 311, 425
- Bruzual A., G. 1983, *ApJ*, 273, 105
- Bruzual, G., & Charlot, S. 2003, *MNRAS*, 344, 1000
- Bundy, K., Bershady, M. A., Law, D. R., et al. 2015, *ApJ*, 798, 7
- Cardelli, J. A., Clayton, G. C., & Mathis, J. S. 1988, *ApJ*, 329, L33
- Chabrier, G. 2003, *PASP*, 115, 763
- Charlot, S., Worthey, G., & Bressan, A. 1996, *ApJ*, 457, 625
- Chen, X. Y., Liang, Y. C., Hammer, F., Zhao, Y. H., & Zhong, G. H. 2009, *A&A*, 495, 457
- Cid Fernandes, R., González Delgado, R. M., Schmitt, H., et al. 2004, *ApJ*, 605, 105
- Cid Fernandes, R., González Delgado, R. M., Storchi-Bergmann, T., Martins, L. P., & Schmitt, H. 2005a, *MNRAS*, 356, 270
- Cid Fernandes, R., Mateus, A., Sodré, L., Stasińska, G., & Gomes, J. M. 2005b, *MNRAS*, 358, 363
- Cid Fernandes, R., Stasińska, G., Schlickmann, M. S., et al. 2010, *MNRAS*, 403, 1036
- Comerford, J. M., Gerke, B. F., Stern, D., et al. 2012, *ApJ*, 753, 42
- Comerford, J. M., Pooley, D., Barrows, R. S., et al. 2015, *ApJ*, 806, 219
- Comerford, J. M., Nevin, R., Stemo, A., et al. 2018, *ApJ*, 867, 66
- Dobos, L., Csabai, I., Yip, C.-W., et al. 2012, *MNRAS*, 420, 1217

- Du, B., Luo, A.-L., Kong, X., et al. 2016, *ApJS*, 227, 27
- Emsellem, E., Cappellari, M., Krajnović, D., et al. 2007, *MNRAS*, 379, 401
- Faber, S. M. 1972, *A&A*, 20, 361
- Fernandes, R. C., Leão, J. R. S., & Lacerda, R. R. 2003, *MNRAS*, 340, 29
- Fischer, T. C., Crenshaw, D. M., Kraemer, S. B., et al. 2011, *ApJ*, 727, 71
- Fu, H., Yan, L., Myers, A. D., et al. 2012, *ApJ*, 745, 67
- Ge, J.-Q., Hu, C., Wang, J.-M., Bai, J.-M., & Zhang, S. 2012, *ApJS*, 201, 31
- Gelderman, R. 1994, *Bulletin of the American Astronomical Society*, 26, 1356
- Hopkins, P. F., Hernquist, L., Martini, P., et al. 2005, *ApJ*, 625, L71
- Kauffmann, G., Heckman, T. M., Tremonti, C., et al. 2003, *MNRAS*, 346, 1055
- Kewley, L. J., Dopita, M. A., Sutherland, R. S., Heisler, C. A., & Trevena, J. 2001, *ApJ*, 556, 121
- Kewley, L. J., Groves, B., Kauffmann, G., & Heckman, T. 2006, *MNRAS*, 372, 961
- Koski, A. T. 1978, *ApJ*, 223, 56
- Kuntschner, H., Emsellem, E., Bacon, R., et al. 2010, *MNRAS*, 408, 97
- Le Borgne, J.-F., Bruzual, G., Pelló, R., et al. 2003, *A&A*, 402, 433
- Le Borgne, D., Rocca-Volmerange, B., Prugniel, P., et al. 2004, *A&A*, 425, 881
- Liu, X., Shen, Y., Strauss, M. A., et al. 2010, *ApJ*, 708, 427
- Liu, X., Civano, F., Shen, Y., et al. 2013, *ApJ*, 762, 110
- Luo, A.-L., Zhao, Y.-H., Zhao, G., et al. 2015, *Research in Astronomy and Astrophysics*, 15, 1095
- Mallmann, N. D., Riffel, R., Storchi-Bergmann, T., et al. 2018, *MNRAS*, 478, 5491
- Mateus, A., Sodr e, L., Cid Fernandes, R., et al. 2006, *MNRAS*, 370, 721
- M uller-S anchez, F., Comerford, J. M., Nevin, R., et al. 2015, *ApJ*, 813, 103
- Nevin, R., Comerford, J., M uller-S anchez, F., Barrows, R., & Cooper, M. 2016, *ApJ*, 832, 67
- Nevin, R., Comerford, J. M., M uller-S anchez, F., Barrows, R., & Cooper, M. C. 2018, *MNRAS*, 473, 2160
- Rosario, D. J., Shields, G. A., Taylor, G. B., Salviander, S., & Smith, K. L. 2010, *ApJ*, 716, 131
- S anchez, S. F., Kennicutt, R. C., Gil de Paz, A., et al. 2012, *A&A*, 538, A8
- Schmitt, H. R., Bica, E., & Pastoriza, M. G. 1996, *MNRAS*, 278, 965
- Schlegel, D. J., Finkbeiner, D. P., & Davis, M. 1998, *ApJ*, 500, 525
- Shen, Y., Liu, X., Greene, J. E., & Strauss, M. A. 2011, *ApJ*, 735, 48
- Smith, K. L., Shields, G. A., Bonning, E. W., et al. 2010, *ApJ*, 716, 866
- Springel, V., Di Matteo, T., & Hernquist, L. 2005, *MNRAS*, 361, 776
- Stasińska, G., Vale Asari, N., Cid Fernandes, R., et al. 2008, *MNRAS*, 391, L29
- Tinsley, B. M. 1978, *ApJ*, 222, 14
- Valdes, F., Gupta, R., Rose, J. A., Singh, H. P., & Bell, D. J. 2004, *ApJS*, 152, 251
- Van Wassenhove, S., Volonteri, M., Mayer, L., et al. 2012, *ApJ*, 748, L7
- Vaughan, S. P., Davies, R. L., Zieleniewski, S., & Houghton, R. C. W. 2018, *MNRAS*, 479, 2443
- Vazdekis, A., & Arimoto, N. 1999, *ApJ*, 525, 144
- Wang, J.-M., Chen, Y.-M., Hu, C., et al. 2009, *ApJ*, 705, L76
- Wang, L.-L., Luo, A.-L., Shen, S.-Y., et al. 2018, *MNRAS*, 474, 1873
- Wang, M.-X., Luo, A.-L., Song, Y.-H., et al. 2019, *MNRAS*, 482, 1889
- York, D. G., Adelman, J., Anderson, J. E., Jr., et al. 2000, *AJ*, 120, 1579
- Yu, Q., Lu, Y., Mohayaee, R., & Colin, J. 2011, *ApJ*, 738, 92